

Influence of polymer bidispersity on the effective particle-particle interactions in polymer nanocomposites

Gianmarco Munaò^{1,*}, Antonio De Nicola², Florian Müller-Plathe³, Toshihiro Kawakatsu⁴, Andreas Kalogirou³, and Giuseppe Milano^{1,2}

¹*Dipartimento di Chimica e Biologia, Università di Salerno, Via Giovanni Paolo II, 132, I-84084, Fisciano (SA), Italy.*

²*Department of Organic Materials Science, Yamagata University, 4-3-16 Jonan Yonezawa, Yamagata-ken 992-8510, Japan.*

³*Eduard-Zintl-Institut für Anorganische und Physikalische Chemie and Center of Smart Interfaces, Technische Universität Darmstadt, Alarich-Weiss-Str. 8, 64287 Darmstadt, Germany.*

⁴*Department of Physics, Tohoku University, Aoba, Aramaki, Aoba-ku, Sendai, Miyagi 980-8578, Japan.*

E-mail: gmunao@unisa.it

Abstract

We investigate the role played by the bidispersity of polymer chains on the local structure and the potential of mean force (PMF) between silica nanoparticles (NPs) in a polystyrene melt. We use the hybrid particle-field molecular dynamics technique which allows to efficiently relax polymer nanocomposites even with high molecular weights. The NPs we investigate are either bare or grafted with polystyrene chains immersed in

a melt of free polystyrene chains, whereas the grafted and the free polystyrene chains are either monodisperse or bidisperse. The two-body PMF shows that a bidisperse distribution of free polymer chains increases the strength of attraction between a pair of ungrafted NPs. If the NPs are grafted by polymer chains, the effective interaction crucially depends on bidispersity and grafting density of the polymer chains: for low grafting densities, the bidispersity of both free and grafted chains increases the repulsion between the NPs, whereas for high grafting densities we observe two different effects. An increase of bidispersity in free chains causes the rise of the repulsion between the NPs, while an increase of bidispersity in grafted chains promotes the rise of attraction. Additionally, a proper treatment of multi-body interactions improves the simpler two-body PMF calculations, in both unimodal and bimodal cases. We found that, by properly tuning the bidispersity of both free and grafted chains, we can control the structure of the composite materials, which can be confirmed by experimental observations. As a results, the hybrid particle-field approach is confirmed to be a valid tool for reproducing and predicting microscopic interactions, which determine the stability of the microscopic structure of the composite in a wide range of conditions.

Introduction

A proper control of microscopic structural arrangements and interactions between components is crucial in order to design a polymer nanocomposite material with specific macroscopic properties. In this context, it has been well documented¹⁻³ that nanoparticles (NPs) dispersed in a polymer matrix tend to aggregate. Such a tendency depends on the NP size, the molecular weight of polymer chains and the NP concentration. Since superior mechanical properties of the composite material can be obtained if the fillers are dispersed, rather than forming aggregates, the NPs are often grafted with polymer chains. In this case, the grafted polymer chains can be either the same chemical species as the polymer in the matrix or different species. On the other hand, experiments⁴⁻⁷ have largely proved that grafted NPs

can be either well dispersed or arranged in nanoaggregates. The onset of a given morphology depends on both the ratio between the molecular weights of free and grafted polymer chains and the grafting density.⁸ Since the interaction between the polymer chains is essential to determine the phase behavior of the composite, a desired morphology can be obtained also by properly tuning the polydispersity of the polymer chains. In recent years, many experimental⁹⁻¹³ as well as theoretical and simulation works¹⁴⁻²⁰ have been devoted to the investigation of the role played by the polydispersity in the characterization of the phase behavior and the stability of nanocomposites. Experimental studies⁹⁻¹³ have shown that if free and grafted polymer chains belong to the same chemical species, NPs with a unimodal distribution of grafted chains tend to aggregate, provided that the molecular weight of the grafted chains is lower than that of the free chains. On the other hand, by mixing short and long grafted chains, the interparticle attraction can be lowered considerably, generating a well dispersed condition. More specifically, much interest is dedicated to low grafting densities, since in this case complex self-assembled nanostructures can be expected.^{1,2} A recent experimental work¹¹ on silica NPs in a polystyrene (PS) matrix, has shown that for low grafting density, in comparison with the monodisperse case, a proper choice of the polydispersity of the grafted chains can enlarge the stable region of the well-dispersed NP phase while makes the self-assembled phase narrow. At the same time, the authors showed that the polydispersity can be used to obtain a desired structure as well, whereas different aggregates appear for unimodal distributions of grafted chains. Simulation studies^{15-17,20} have proved that the attractive or repulsive behavior of the effective interactions (and hence the onset of aggregates) is due to the wettability of the NP surfaces with the free polymers, which, in turn, depends on the local structure of polymer chains. An accurate description of the chain arrangements in proximity of the NP surface and the interaction between free and grafted chains is crucial to predict the final behavior of the composite. However the understanding of these mechanisms at a molecular level is not straightforward, due to the number of interactions that should be taken under control. In order to overcome these issues, many simulation studies

of silica NPs in a PS melt have been performed. More specifically, structure and dynamics in the melt state and elastic constants in the glassy state of systems consisting of bare silica NPs immersed in long-chain polystyrene matrices have been simulated in Ref.²¹ Structure around a silica NP bearing surface grafted polystyrene chains in a molten polystyrene matrix has been explored in Ref.²² while a similar study for bare nanoparticles has been conducted in Ref.²³

Despite the large number of studies carried out so far, there are still questions that need to be addressed: from a simulation point of view, it is worth pointing out that generally only non-specific bead-spring polymer models and hard spheres for NPs have been adopted, which disregard information on the chemical nature of the nanocomposites. A further point concerns the importance of contributions to the total interaction from the three-body (or, in general, multi-body) effects. This is particularly true in cases of polymer chains with high molecular weight, where a single chain can easily interact with more than two NPs, hence making the multi-body contributions not negligible, as shown in recent simulations²⁴ and theoretical²⁵ works.

We propose a simulation study of the two-body and three-body potentials of mean force (PMF) among 2 or 3 silica NPs (bare or grafted with PS chains) embedded in a PS matrix. We adopt the hybrid particle-field molecular dynamics approach²⁶ which has been recently employed to efficiently characterize, among others, nanocomposites,^{24,27,28} polymer melts of high molecular weight²⁹ and carbon nanotubes.³⁰ In addition, a number of studies have been devoted to capture structure, thermodynamics, and also entangled polymer dynamics of polymer melts in the bulk and at interfaces.³¹⁻³⁴ The advantage to use a hybrid approach relies on the possibility to significantly speed up the simulation time typically required to get a proper relaxation of polymer nanocomposites.²⁹ This speed up is achieved by decoupling the mutual particle-particle interactions and replacing them with a field representation. According to the hybrid approach the density fields are obtained by calculating “on the fly” the density values from the particle positions. This prescription allows us to perform realistic

simulations of systems with a molecular/atomistic detail, with applications to polymers,^{29,35} biological models like phospholipids,³⁶ proteins³⁷ and systems for drug release.³⁸ In addition, this scheme paves the way to the study of equilibrium properties (like the PMF), whose treatment with traditional simulation approach is difficult.²⁴ In the present work the grafting density and the polydispersity of both free and grafted polymer chains are varied, and realistic coarse-grained (CG) models are needed, which have to account for the chemical detail of the system. We consider two different molecular weights of polymer chains, *i.e.* we use a bidisperse system. In order to ascertain the role played by free and grafted chains, we separately investigate the effects of the bidispersity of both of these two types of chains.

Simulation protocol

The models for silica NPs and for PS chains, together with a proposed simulation method, have been already adopted to successfully investigate monodisperse systems.^{24,28} All details concerning these models and the relative simulation strategies can be found in those works and in references therein, although their general description is reported in the following subsections.

Coarse-grained models and hybrid particle-field approach

The CG models adopted in the present work have been developed by Qian and coworkers³⁹ and successfully implemented in Refs.^{24,28,40} In the CG model of atactic PS, a repeating unit is replaced by a single bead placed at its center of mass. Bond length, angle, dihedral and torsional parameters are set in order to reproduce the local structure of atomistic PS models. Also, two different kinds of beads account for the chirality of the asymmetric carbon. In the CG model of the NP a single bead is centered on the silicon atom position and represents one SiO₂ unit. The total mass of the surface hydrogen atoms is distributed over all the beads of the NP. The simulated NP has a diameter of 4 nm and contains 873 beads. In

addition, we also consider systems where some PS chains are grafted to the NP surface. Following the prescription by Ghanbari and coworkers,⁴⁰ each grafted chain is attached to the NP surface through a linker unit, that is divided into four beads of two kinds with the same mass. Further details on this CG representation and its validation can be found in Refs.^{28,40} In those works it has been demonstrated that local structure, gyration radius and spatial orientation of free and grafted chains well reproduce the atomistic models studied in Refs.^{41,42} The latter, in turn, show a good agreement with experiments in describing the structural properties of the polymer in the vicinity of the NP, concerning in particular the layering of the chains and the interfacial properties. In addition, a further validation of our approach has been performed in Ref.²⁴ in which the experimental phase behavior of silica-polystyrene nanocomposites has been qualitatively reproduced by a proper combination of two-body and three-body PMF.

The simulation approach that we adopt in the present work is based on a combination of a standard molecular dynamics (MD) approach and a self-consistent field (SCF) theory⁴³ for the calculation of non-bonded potentials. The resulting scheme is known as hybrid particle-field model:²⁶ in this approach, the Hamiltonian of a system of M molecules is split as:

$$\hat{H}(\Gamma) = \hat{H}_0(\Gamma) + \hat{J}(\Gamma) \tag{1}$$

where Γ represents a point in the phase space and the symbol $\hat{}$ indicates that a given quantity is a function of the microscopic state corresponding to Γ . In Eq. 1, $\hat{H}_0(\Gamma)$ is the Hamiltonian of a system where the molecules experience only intramolecular interactions, whereas $\hat{J}(\Gamma)$ is the contribution due to all non-bonded interactions. The latter can be calculated as an external potential $V(\mathbf{r})$ on single particles, which is due to the density field. The details of the derivation of $V(\mathbf{r})$ can be found elsewhere.²⁶ The mean field solution for

the potential $V_K(\mathbf{r})$ acting on a particle of type K at position \mathbf{r} , is:

$$V_K(\mathbf{r}) = k_B T \sum_{K'} \chi_{KK'} \Phi_{K'}(\mathbf{r}) + \frac{1}{\kappa} \left(\sum_{K'} \Phi_{K'}(\mathbf{r}) - 1 \right) \quad (2)$$

where k_B is the Boltzmann constant, T is the temperature, $\chi_{KK'}$ are the mean field parameters for the interaction of a particle of type K with the density field due to particles of type K' and the second term on the right-hand side of Eq. 2 is the incompressibility condition, κ being the compressibility. Also, $\Phi_K(\mathbf{r})$ and $\Phi_{K'}(\mathbf{r})$ are the density functions of the beads of types K and K' , respectively, and normalized by the bulk density value ϕ_0 . For the NP-PS interactions $\chi_{KK'} \times RT = 5.25$ kJ/mol (R being the gas constant), while for NP-NP and PS-PS interactions $\chi_{KK'} \times RT = 0$, in agreement with a previous MD-SCF study of the same model.²⁸

All simulations have been performed by means of the OCCAM code, whose details can be found in Ref.,⁴⁴ and run in the NVT ensemble, with the temperature (fixed at 590 K) controlled by the Andersen thermostat and a time step of 4 fs. The density fields, with the corresponding derivatives, are calculated on a lattice obtained by dividing the simulation box into a grid of cells, whose spacing has been set to 1.18 nm. The density is calculated from particle positions and projected on the mesh according to a procedure described in Ref.²⁸ The mesh is updated every 100 MD time steps. The initial configurations have been built by using the Packmol program.⁴⁵ All particles have been enclosed in a simulation box with periodic boundary conditions: box sizes, along with the number of particles simulated, are reported in Tabs. 1 and 2. The total force acting on each particle is a sum of intramolecular interactions (obtained by means of tabulated potentials) and contributions due to its interactions with the density fields. The latter is interpolated from the density values at the mesh points.⁴⁴ Finally, we point out that, as observed in previous works on similar systems,^{24,28} in principle the incompressibility condition could cause the unphysical presence of PS chains inside the NP. In order to avoid this effect, the NP density is modelled by an analytical effective field,

following a prescription reported in Ref.⁴⁶ Specifically, the NP density field is represented by a combination of two spline functions, one describing the density field inside the NP core and the other preventing the external chains from overlapping the NP. These functions are calculated by fixing four parameters: the NP radius r_0 , the core density ϕ_{core} , the surface density ϕ_{max} and the interval δr giving the width of the NP density profile (*i.e.* how fast the NP density field goes from ϕ_{max} at $r = r_0$ to zero at $r = r_0 + \delta r$). In our model we set the same parameters reported in Ref.,²⁴ namely $r_0 = 2$, $\phi_{core} = 100$, $\phi_{max} = 2$ and $\delta r = 0.50$. The spline coefficients are then obtained by imposing the continuity of the NP density and its derivative.

Two- and three-body potentials of mean force

For the calculation of the two-body PMF between two NPs, for each system we have prepared a set of 30 independent initial configurations, each one corresponding to a pair of NPs placed at a fixed distance d from each other and embedded in the polymer matrix. A single simulation run has been performed from each starting configuration, where the NPs were allowed to freely rotate but not to translate, in order to keep their distance fixed. Forces $\bar{F}(d)$ on the centers of mass of the two NPs have been computed at every 0.4 ps and the convergence has been ensured by verifying that the average values of the forces do not change anymore up to the first significant digit. During the calculation of the two-body PMF, after a first simulation run of at least 60 ns, forces have been averaged over a subsequent production stage covering the same amount of time. If not explicitly reported in the figures, error bars corresponding to standard deviations are smaller than symbol sizes of the corresponding curves. The resulting PMF has been calculated according to the equation:

$$W(d) = - \int_d^\infty \bar{F}(r) dr, \tag{3}$$

where r is the interparticle distance, ranging in the $[d_{\min}, d_{\max}]$ interval. In our simulations, $d_{\min} = 4$ nm and $d_{\max} = 10$ nm; therefore d_{\min} is coincident with the NP diameter, while d_{\max} indicates an interparticle distance where the potential can be confidently assumed equal to zero. This d_{\max} is also used as the practical infinity in Eq. 3. In all simulations, distances are sampled with a step of 0.2 nm and the numerical integration is performed by employing the trapezoidal rule.

The procedure for calculating the three-body PMF requires a slightly different approach: in this case the system is prepared including three NPs at fixed distance from each other and surrounded by polymer chains. In analogy with the two-body case, we increase the distance d between the first two NPs, leaving the position of the third NP unchanged, and then we compute the forces experienced by them. The three-body contribution to the resulting PMF is maximum if the third NP is close to the others. In principle, also the distance D between the third NP and the midpoint of the line joining the first two NPs can be increased: this allows us to estimate the short-range or long-range nature of the three-body interaction. Since we are interested in the computation of this interaction when the third NP is close to the first two (when these effects are stronger) in our simulations we have kept D fixed to 4 nm. The whole procedure is schematically represented in Fig. 1. In the calculation of the three-body PMF, the convergence has been achieved after typically 120 ns and the forces have been averaged over a production run of 60 ns.

System preparation

Since the effective interactions between NPs are mediated by the interactions with polymer chains, the calculation of the PMF has been systematically supported by simulations of systems comprising a single NP (ungrafted or grafted) in a PS matrix, which contains polymer chains of different lengths. In a previous work²⁴ we have investigated the role played by the molecular weight of monodisperse free and grafted chains on the NP-NP interactions. In the present work we focus on the role played by bidispersity and grafting density. For such an

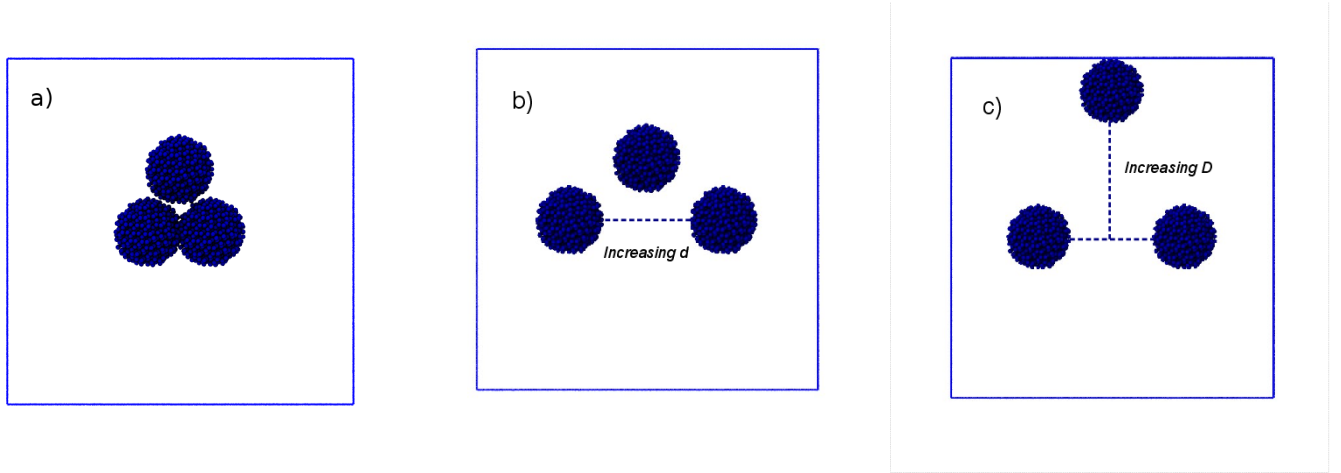


Figure 1: Schematic procedure for the calculation of the three-body potential of mean force: starting from a configuration where all nanoparticles are in close contact (a), the distance d between the first two nanoparticles increases, leaving unchanged the position of the third nanoparticle (b). The short or long-range nature of the three-body potential of mean force can be determined by increasing the distance D between the third nanoparticle and the center of the line joining the centers of mass of the first two nanoparticles (c).

aim we have introduced a bidispersity index (BDI) defined as:

$$BDI = M_w/M_n \quad (4)$$

where M_w and M_n are the weight average molecular weight and the number average molecular weight, respectively, and are defined as:

$$M_w = \frac{\sum_i N_i M_i^2}{\sum_i N_i M_i}, \quad M_n = \frac{\sum_i N_i M_i}{\sum_i N_i}, \quad (5)$$

where N_i and M_i indicate the number of chains with a given molecular weight and the number of beads belonging to each of these chains. The systems are listed in Tab. 1, along with the grafting densities, the number and molecular weight of free and grafted chains and two different bidispersity indices BDI_f and BDI_g , which take into account the bidispersity of free and grafted chains, respectively.

Table 1: Nanocomposite systems constituted by a single nanoparticle in a polystyrene matrix. The grafting density ρ_g is in unit of chains/nm². The box lengths are $L_x = L_y = L_z = 15.74$ nm. The chain length is given in number of beads. BDI_f and BDI_g are the bidispersity indices of free and grafted chains, respectively.

| ρ_g | No° of short grafted chains | No° of long grafted chains | Short grafted chains length | Long grafted chains length | No° of short free chains | No° of long free chains | Short free chains length | Long free chains length | BDI_g | BDI_f |
|----------|-----------------------------|----------------------------|-----------------------------|----------------------------|--------------------------|-------------------------|--------------------------|-------------------------|---------|---------|
| 0 | 0 | 0 | 0 | 0 | 1070 | 0 | 20 | 0 | 0 | 1 |
| 0 | 0 | 0 | 0 | 0 | 840 | 23 | 20 | 200 | 0 | 2.36 |
| 0 | 0 | 0 | 0 | 0 | 100 | 19 | 20 | 1000 | 0 | 5.14 |
| 0.1 | 0 | 5 | 0 | 80 | 1070 | 0 | 20 | 0 | 1 | 1 |
| 0.1 | 0 | 5 | 0 | 80 | 840 | 23 | 20 | 200 | 1 | 2.36 |
| 0.1 | 0 | 5 | 0 | 80 | 100 | 19 | 20 | 1000 | 1 | 5.14 |
| 0.1 | 1 | 4 | 10 | 80 | 1005 | 0 | 20 | 0 | 2.36 | 1 |
| 0.1 | 1 | 4 | 5 | 80 | 1007 | 0 | 20 | 0 | 3.25 | 1 |
| 0.5 | 0 | 25 | 0 | 80 | 877 | 0 | 20 | 0 | 1 | 1 |
| 0.5 | 0 | 25 | 0 | 80 | 177 | 69 | 20 | 200 | 1 | 2.36 |
| 0.5 | 0 | 25 | 0 | 80 | 84 | 16 | 20 | 1000 | 1 | 5.14 |
| 0.5 | 5 | 20 | 10 | 80 | 991 | 0 | 20 | 0 | 2.36 | 1 |
| 0.5 | 5 | 20 | 5 | 80 | 1001 | 0 | 20 | 0 | 3.25 | 1 |

The total collection of investigated systems for the calculation of the two-body PMF is reported in Tab. 2: note that in this case the simulation box is not cubic but is elongated along the direction joining the centers of the two NPs. In all bidisperse systems the polymer density is equal (or very close) to that of monodisperse cases. However, since the chains (free or grafted) follow a bimodal distribution, the number average molecular weight M_n (see Eq. 5) is not the same as in the unimodal case. For bidisperse free chains this circumstance is not expected to influence the two-body PMF, in agreement with recent simulation²⁴ and theoretical⁴⁷ studies where it has been demonstrated that the two-body PMF is weakly dependent on the molecular weight of the free chains M_n . For bidisperse grafted chains we have first kept the M_n constant, in order to limit the effects only due to the bidispersity. Then, also M_n has been varied, allowing us to explore a large variety of behaviors. We have verified that the radius of the NP (corresponding to 2 nm) is equivalent to the gyration

Table 2: Nanocomposite systems investigated for the calculation of the two-body potential of mean force. The grafting density ρ_g is in unit of chains/nm². The box lengths are $L_x = 22$ nm, $L_y = L_z = 12.5$ nm. The chains length is given in number of beads.

| ρ_g | No ^o of short grafted chains | No ^o of long grafted chains | Short grafted chains length | Long grafted chains length | No ^o of short free chains | No ^o of long free chains | Short free chains length | Long free chains length | BDI_g | BDI_f |
|----------|---|--|-----------------------------|----------------------------|--------------------------------------|-------------------------------------|--------------------------|-------------------------|---------|---------|
| 0 | 0 | 0 | 0 | 0 | 1044 | 0 | 20 | 0 | 0 | 1 |
| 0 | 0 | 0 | 0 | 0 | 300 | 75 | 20 | 200 | 0 | 2.36 |
| 0 | 0 | 0 | 0 | 0 | 950 | 2 | 20 | 1000 | 0 | 5.14 |
| 0.1 | 0 | 5 | 0 | 80 | 995 | 0 | 20 | 0 | 1 | 1 |
| 0.1 | 0 | 5 | 0 | 80 | 840 | 23 | 20 | 200 | 1 | 2.36 |
| 0.1 | 0 | 5 | 0 | 80 | 100 | 19 | 20 | 1000 | 1 | 5.14 |
| 0.1 | 3 | 2 | 13 | 180 | 995 | 0 | 20 | 0 | 2.00 | 1 |
| 0.1 | 4 | 1 | 10 | 80 | 1005 | 0 | 20 | 0 | 2.36 | 1 |
| 0.1 | 4 | 1 | 5 | 80 | 1007 | 0 | 20 | 0 | 3.25 | 1 |
| 0.1 | 4 | 1 | 80 | 1000 | 903 | 0 | 20 | 0 | 2.94 | 1 |
| 0.5 | 0 | 25 | 0 | 80 | 854 | 0 | 20 | 0 | 1 | 1 |
| 0.5 | 0 | 25 | 0 | 80 | 187 | 69 | 20 | 200 | 1 | 2.36 |
| 0.5 | 0 | 25 | 0 | 80 | 84 | 16 | 20 | 1000 | 1 | 5.14 |
| 0.5 | 20 | 5 | 40 | 240 | 854 | 0 | 20 | 0 | 2.00 | 1 |
| 0.5 | 20 | 5 | 10 | 80 | 991 | 0 | 20 | 0 | 2.36 | 1 |
| 0.5 | 20 | 5 | 5 | 80 | 1001 | 0 | 20 | 0 | 3.25 | 1 |

radius of chains containing 80 beads.²⁴ Hence, the mean size of the longest chains simulated (containing 1000 beads) is considerably larger than the size of a single NP.

The total interaction between the pair of NPs has two contributions: the first is the direct interaction among the NP cores, which is modeled by a Hamaker potential,⁴⁸ parameterized on the basis of atomistic simulations in Ref.⁴⁹ Specifically, in that work the NP-NP interactions were calculated for ungrafted silica NPs of different sizes; in all cases the Hamaker potential was found to agree very well with the atomistic simulations, indicating that it accurately reproduces the NP core-core attractive interaction. The second contribution to the total interaction is given by the surrounding polymer chains, calculated by performing molecular simulations according to the procedure described in Section **Two- and three-body potentials of mean force**. More details on this approach, successfully applied to

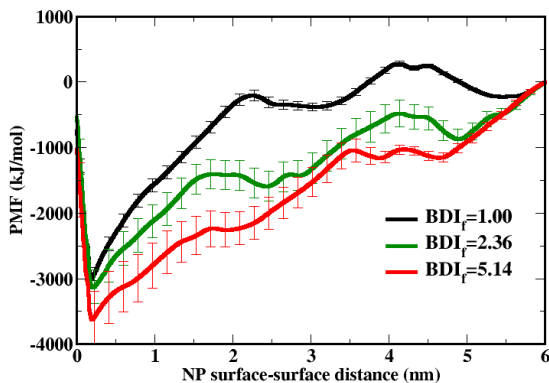


Figure 2: Effect of increasing the bidispersity index of the free chains on the potential of mean force between two ungrafted nanoparticles.

silica-polystyrene nanocomposites with monodisperse PS chains, can be found in Refs.^{24,49} In order to discriminate between the effects due to the bidispersity of free and grafted chains, as well as on the different behaviors between ungrafted and grafted NPs, we have separately discussed these cases in different subsections.

Results and discussion

Increasing the bidispersity of free chains: the ungrafted case

The PMF between a pair of ungrafted NPs for different BDI_f is reported in Fig. 2: for the monodisperse case (black line), the effective interaction is remarkably attractive, as already observed in Ref.²⁴ The attraction, in particular at shorter NP-NP distance, is due to the chain confinement, since only a small number of chains with elongated conformations fit between the two NPs. Conversely, for larger interparticle separations, a progressively higher number of free chains can be arranged therein until this number becomes comparable with the bulk and the attraction vanishes. The increase of the bidispersity of free chains, obtained by mixing short (20 beads) and long (200 and 1000 beads, see Tab. 2) chains

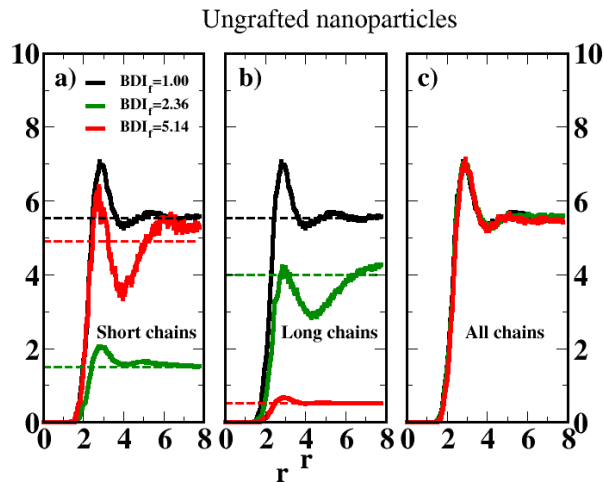


Figure 3: Monomer number density of polymer chains as a function of their distance from the center of an ungrafted nanoparticle upon increasing the bidispersity index of the free chains. Short (a), long (b) and all (c) chains are separately reported. Broken horizontal lines indicate the density levels that would correspond to the short and long chains if the mixture was homogeneous.

leads to a slight increase of the attraction between the NPs. In addition, we note that the oscillating behavior, observed for $BDI_f = 1$ is progressively suppressed. The physical length which governs the wavelength of the oscillations is the NP radius.²⁴ As explained in previous theoretical^{25,47,50} and simulation^{24,51} studies, oscillations develop for moderate NP-NP attractions, where the regions of perturbed polymer density around each NP can overlap. The progressive disappearance of the oscillations indicates the breakdown of this mechanism, and the simultaneous onset of a stronger attraction between the NPs. All these effects can be entirely ascribed to the increase of BDI_f since, as previously anticipated, the free chains M_n does not influence the two-body PMF.^{24,47}

In order to provide an explanation of the increase of the attraction with the bidispersity, we have investigated the arrangement of short and long chains around a single NP by calculating their monomer number density for different values of BDI_f . Results are reported in Fig. 3: in particular, we separately show the cases corresponding to short (panel (a)), long (panel (b)) and all (panel (c)) chains. It is worth pointing out that long chains comprise 200

beads if $BDI_f = 2.36$ and 1000 beads if $BDI_f = 5.14$ (see Tab. 1). The monomer number density for the monodisperse case exhibits the maximum value for a distance from the NP center of ≈ 3 nm, followed by the minimum value and the second maximum for a distance of ≈ 5 nm, finally converging to its bulk value. The first peak in the monomer number density of short chains is still observed for $BDI_f=2.36$ and the density profile becomes even more structured for $BDI_f=5.14$. This trend is reversed for the long chains (panel (b)), with the density profile becoming progressively less structured upon increasing BDI_f . The exchange in the order of short and long chains is undoubtedly a consequence of the different numbers of monomers belonging to the two kinds of chains, but nevertheless the emerging picture (suggesting a shell structure, with the short chains arranged close to the NP surface and the long chains around them) seems genuine. The broken horizontal lines shown in panels (a) and (b) indicate the density values corresponding to homogeneous distributions of short and long chains. The monomer number densities of both short and long chains do not attain their homogeneous values even for distances from the NP center as large as 8 nm. In comparison with a multiscale simulation study of PS-SiO₂ nanocomposites,²¹ where a layering of monodisperse chains was observed, in our study the chain layering extends until higher distances from the NP surface. This effect can be ascribed to the bidispersity in the chain length. In addition, if we consider the collective contribution given by short and long chains together (panel (c)) we find no effects due to BDI_f : this suggests that the structuring of the number density for short chains is compensated by the decrease of that for long chains and vice versa. In order to quantify the difference of the chain arrangements around the NP surface, we have calculated the Gibbs free energy $\Delta G(r)$ for the replacement of a monomer of a short chain with that of a long chain in the coordination environment of a short chains, following the prescription reported in Ref.:⁵²

$$\ln \frac{g_{\text{long}}(r)}{g_{\text{short}}(r)} = \frac{-\Delta G(r)(\text{short} \rightarrow \text{long})}{RT}, \quad (6)$$

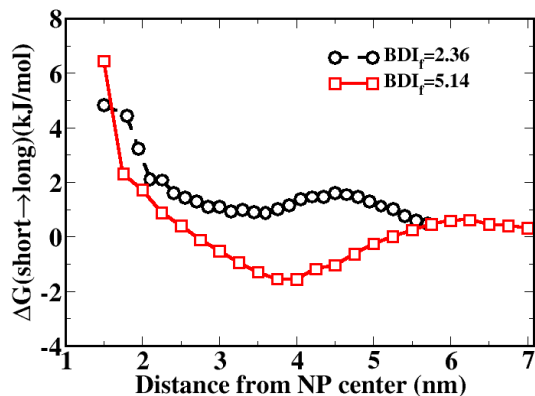


Figure 4: Gibbs free energy for the exchange of a monomer belonging to a short free chain with a monomer belonging to a long free chain as a function of the distance between the chains and the center of a ungrafted nanoparticle. Two different bidispersity indices of the free chains (reported in the legend) are considered.

where $g_{\text{short}}(r)$ and $g_{\text{long}}(r)$ are the two radial distribution functions for monomers belonging to short and long chains around the NP, respectively, and r is the distance from the NP center. In Fig. 4 we report the values of $\Delta G(r)(\text{short} \rightarrow \text{long})$ for $BDI_f = 2.36$ and 5.14: in both cases $\Delta G(r)$ is strictly positive in proximity of the NP surface. Upon increasing the distance, for $BDI_f = 2.36$ $\Delta G(r)$ remains positive, whereas for $BDI_f = 5.14$ the minimum is found when the distance from the NP center is 4 nm. We also note that, due to the softness of the NP-PS interaction, $\Delta G(r)$ shows non-zero values also for distances from the NP center less than the NP radius. A similar behavior was also observed in a simulation study of a CG model for athermal all-polystyrene nanocomposite:²³ in particular, the authors observed that when the radius of gyration of chains is comparable in size to the nanoparticle the centers of mass of the chains may penetrate the interior of the NP, as chains engulf the NP. According to the picture provided by Figs. 3-4, it emerges that, when the PS chains are bidisperse, replacing a monomer belonging to short chain with one belonging to a long chain carries a Gibbs free energy penalty; hence there is a tendency of short chains to be arranged close to the NP surface, with the long chains just outside this first shell. If two NPs come in close contact (see Fig. 2) this configuration can no longer be realized, since the long chains can not

be arranged in the narrow space between the NPs. As a consequence, each NP has to “desorb” short chains from the first shell, in order to put them at the interface with the other NP. This desorption causes the increase of the attraction between the NPs upon increasing BDI_f . This picture can be qualitatively confirmed by comparing the number of monomers belonging to short and long chains around a single “unperturbed” NP with that found when two NPs come in close contact. The difference in the composition of the first shell (from 0 to 0.5 nm from the NP surface) around the NP of monomers belonging to short and long chains can be estimated; for $BDI_f = 2.36$ the number of monomers belonging to short and long chains changes from 74 and 12 for a single NP to 18 and 53 for a pair of NPs. Similarly, this number changes from 67 and 10 to 9 and 70 for $BDI_f = 5.14$. Hence, there are 103 substitutions in the first case and 118 in the second case; by multiplying these values for $\Delta G(r)$ we obtain 463 kJ/mol for $BDI_f = 2.36$ and 767 kJ/mol for $BDI_f = 5.14$, which qualitatively follows the increase of the attraction between the two NPs. Interestingly, a similar behavior is described in Ref.,¹⁸ where the authors investigate the effect of the increase of BDI_f on the effective interactions between grafted NPs. In their case the molecular weight of the grafted chains is systematically lower than that of free chains, regardless of their bidispersity; as a consequence, the resulting interaction is attractive since in all cases the length of the free chains is higher than the length of the grafted chains.^{8,16,53} The authors observe that short chains preferentially wet the grafted layer in comparison with the long chains, showing a higher correlation with the NPs at short distances. This can be ascribed to an higher gain in the entropy of mixing between grafted and short chains than that between grafted and long chains. Indeed, it is known that for monodisperse systems the wetting of the grafted layer decreases if the length of the free chains increases;^{15,53,54} hence, since the length of the free chains is higher than the length of the grafted chains, short chains preferentially wet the grafted layer more than long chains. In our case the NP is ungrafted and the tendency of short chains to wet the NP surface more than the long chains appears even stronger. The different arrangements of short and long chains around a single ungrafted NP

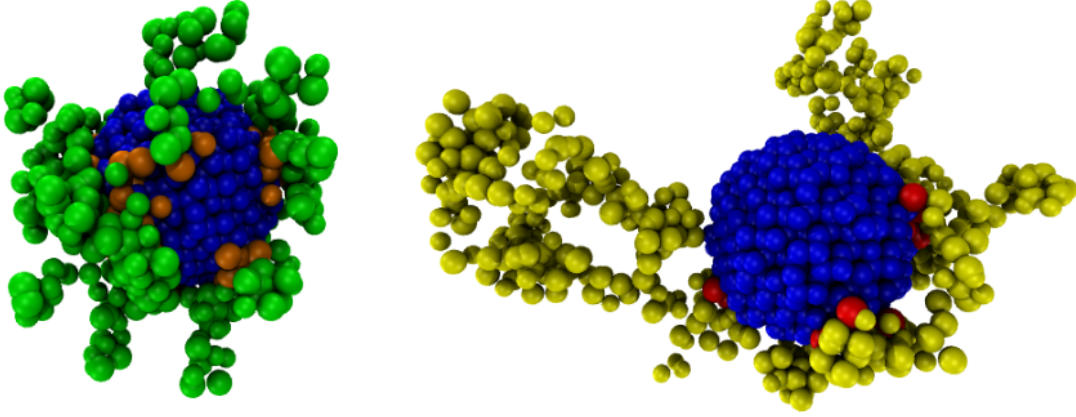


Figure 5: Local arrangements of short (left) and long (right) free chains around a ungrafted NP for a bidispersity index of the free chains set to 2.36. Only chains with at least one bead placed within 0.5 nm from the nanoparticle surface are reported. Short and long chains are depicted in green and yellow, while the beads close to the nanoparticle surface are given in orange and red, respectively.

for $BDI_f = 2.36$ are reported in Fig. 5: more specifically, we show only chains which at least one bead placed within a distance of 0.5 nm from the NP surface. It emerges that there are typically 30 short chains and 3 long chains with 119 and 16 beads close to the NP surface, respectively. Hence, each long chain, on average, has 5.33 beads which fall within 0.5 nm from the NP surface; for short chains this number is 3.96. This means that the long chains are multiply bent when approaching the NP surface and such configurations are entropically unfavoured in comparison to the short chains that do not experience similar arrangements.

We have further characterized the NP-PS interface by calculating the work of adhesion W_{ad} between the PS melt and a single silica NP. In our approach we calculate W_{ad} as:

$$W_{ad} = \frac{\sum_N V_{NP-PS}(\mathbf{r})}{A_{NP}}, \quad (7)$$

where A_{NP} is the surface area of the NP and

$$V_{NP-PS}(\mathbf{r}) = k_B T \chi_{KK'} \Phi_{K'}(\mathbf{r}), \quad (8)$$

which corresponds to the first term of the right hand side of Eq. 2. Taking into account the roughness of the NP surface, we have calculated its area by means of the GROMACS⁵⁵ tool for the solvent access surface area, with a value of r_{probe} corresponding to the radius of a polymer bead (*i.e.* 0.35 nm). By following this prescription we have obtained 90 nm² for the NP area. According to this procedure the work of adhesion is $W_{ad} = 58.89$ mJ/m² for $BDI_f=1.00$, $W_{ad} = 60.55$ mJ/m² for $BDI_f = 2.36$ and $W_{ad} = 67.78$ mJ/m² for $BDI_f = 5.14$. Hence we document a progressively stronger adhesion of PS chains onto the NP surface upon increasing BDI_f . Such estimations satisfactorily agree with the experimental value⁵⁶ of $W_{ad} = 70$ mJ/m² (found for monodisperse systems), especially considering that the proposed CG model has been developed for reproducing the density profiles rather than interfacial properties of silica-PS composites.

Increasing the bidispersity of free chains: the grafted case

Upon grafting the NPs, the scenario significantly changes, as observed by calculating the PMF between a pair of grafted NPs with a grafting density of 0.1 chains/nm² (see Fig. 6a). We first investigate the effects due to the increase of BDI_f , leaving BDI_g unchanged. For the monodisperse case, the PMF is attractive in the whole investigated range of interparticle distances, even if the strength of the attraction is considerably lower than the ungrafted case. This is due to the grafted chains that, as described in our previous work,²⁴ introduce repulsive contributions able to stabilize the whole nanocomposite with respect to the aggregation. Indeed we have shown in the same work that the increase of either the grafting density or the length of the grafted chains improves the miscibility of the NPs with the PS melt. The same behavior was found also in a simulation study of silica-PS nanocomposites²² performed by

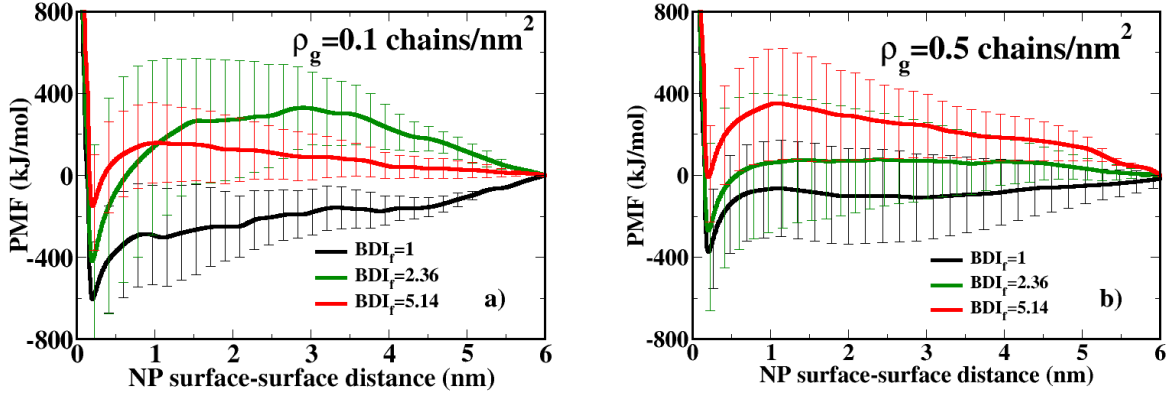


Figure 6: Effect of increasing the bidispersity index of free chains on the potential of mean force between two grafted nanoparticles with grafting density $\rho = 0.1$ (a) and 0.5 (b) chains/nm². In all cases the grafted chains are monodisperse.

means of a Monte Carlo methodology based on polymer mean field theory. Upon increasing BDI_f the repulsion between NPs increases in turn, especially in the intermediate range of interparticle distances. In addition, we note the existence of a crossover between the behaviors of the two bidisperse cases: for interparticle distances closer than 1 nm, the repulsion monotonically increases with BDI_f , whereas for larger distances the repulsion is higher for $BDI_f = 2.36$ than for $BDI_f = 5.14$.

Upon increasing the grafting density to $\rho_g = 0.5$ chains/nm² (Fig. 6b) the two-body PMF similarly behaves: in the unimodal distribution the effective interaction is attractive in the whole range of interparticle separations and becomes progressively more repulsive upon increasing BDI_f . However, in this case the repulsion monotonically increases with the bidispersity, without showing any crossover. Hence, it emerges that the increase of BDI_f favours a good dispersion of the NPs for both the grafting densities.

As previously done for ungrafted NPs, a comparison with the behavior of the monomer number density of free and grafted chains around a single NP can be helpful for understanding the behavior of the effective interactions. In the top panels of Fig. 7 we show the bead number density profiles for $\rho_g = 0.1$ chains/nm²: in comparison with the ungrafted case (see Fig. 3)

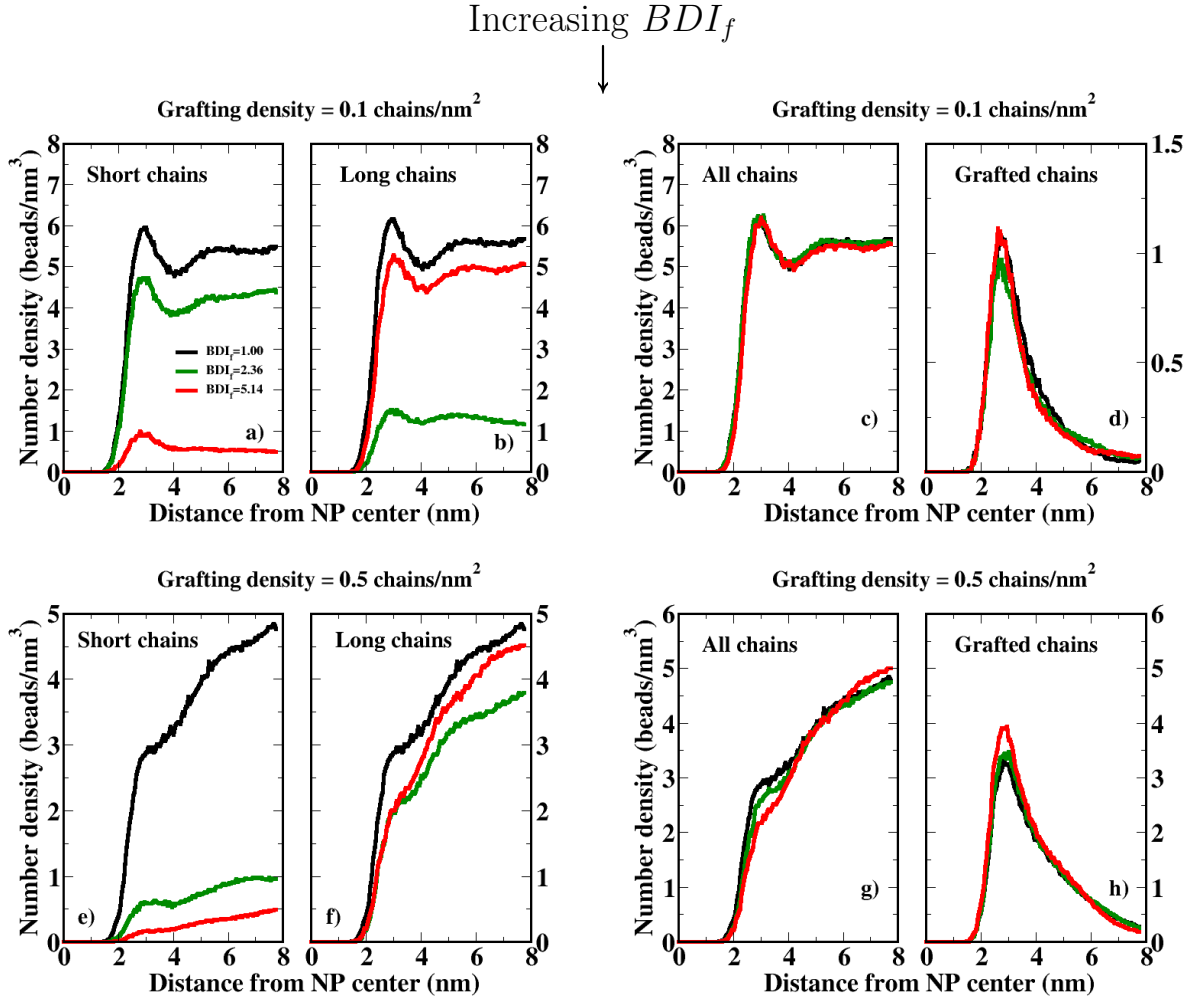


Figure 7: Radial number density of monomers belonging to free and grafted chains. Two different grafting densities, namely $\rho_g = 0.1$ (top panels) and 0.5 (bottom panels) chains/nm² are reported. Short, long and all free chains are separately shown.

the density profiles of both short and long chains oppositely behave upon increasing BDI_f . As a consequence, the two-body PMF is progressively more repulsive: this suggests that, beside the repulsion between grafted chains already existing in the monodisperse case, there is an extra repulsion between grafted chains and the short chains lying at the interface between the two NPs. In order to confirm this assumption, we have checked the behavior of short and long chains by looking at different configurations in proximity of the NPs during the calculations of the two-body PMF; we have verified that for short intermolecular distances, the long chains can hardly be arranged between the two NPs and short chains are

progressively pushed away from the NP surfaces. This behavior is not observed for ungrafted NPs and is due to the repulsive interaction between free and grafted chains. Similar effects have been observed also in simulation studies of atomistic models of silica NPs in a PS^{41,42} or PMMA⁵⁷ melts. It is also worth pointing out that, unlike the systems investigated in Ref.¹⁸ and previously discussed, in this case the length of the free chains is not always higher than the length of the grafted chains: this explains the different PMF observed.

For $\rho_g = 0.5$ chains/nm² (bottom panels of Fig. 7) the profiles of both short and long chains significantly change: because of the higher number of grafted chains, the space available for free chains is substantially reduced, regardless of their molecular weight. Hence, no peak is found in their distributions, which monotonically approach the bulk value. However, the trends of short and long chains upon increasing BDI_f are the same as that observed for $\rho_g = 0.1$ chains/nm² and hence the corresponding two-body PMF (reported in Fig. 6b) are progressively more repulsive for higher bidispersities.

Increasing the bidispersity of grafted chains

We now focus on the effect of increasing BDI_g , leaving BDI_f unchanged. In Fig. 8 we analyze the radial number density of monomers for $\rho_g = 0.1$ (top panels) and 0.5 (bottom panels) chains/nm² upon increasing BDI_g from 1 to 3.25. For $\rho_g = 0.1$ chains/nm² the monomer number densities of short (panel (a)) and long (panel (b)) chains oppositely behave, similarly to the trend observed upon increasing BDI_f . This circumstance suggests that for $\rho_g = 0.1$ chains/nm² the dependence of the two-body PMF on BDI_g is expected to be similar to that observed on BDI_f . In addition, also in this case the global behavior of all grafted chains (panel (c)) and free chains (panel (d)) is not significantly influenced by the bidispersity.

For $\rho_g = 0.5$ chains/nm², the behavior of the monomer number density for short chains (panel (e)) is very similar to that observed for $\rho_g = 0.1$ chains/nm², whereas for long chains (panel (f)) the profiles for $BDI_g = 2.36$ and $BDI_g = 3.25$ are practically coincident. Hence, in this case the decrease of the density profile of short chains is not offset by the increase of

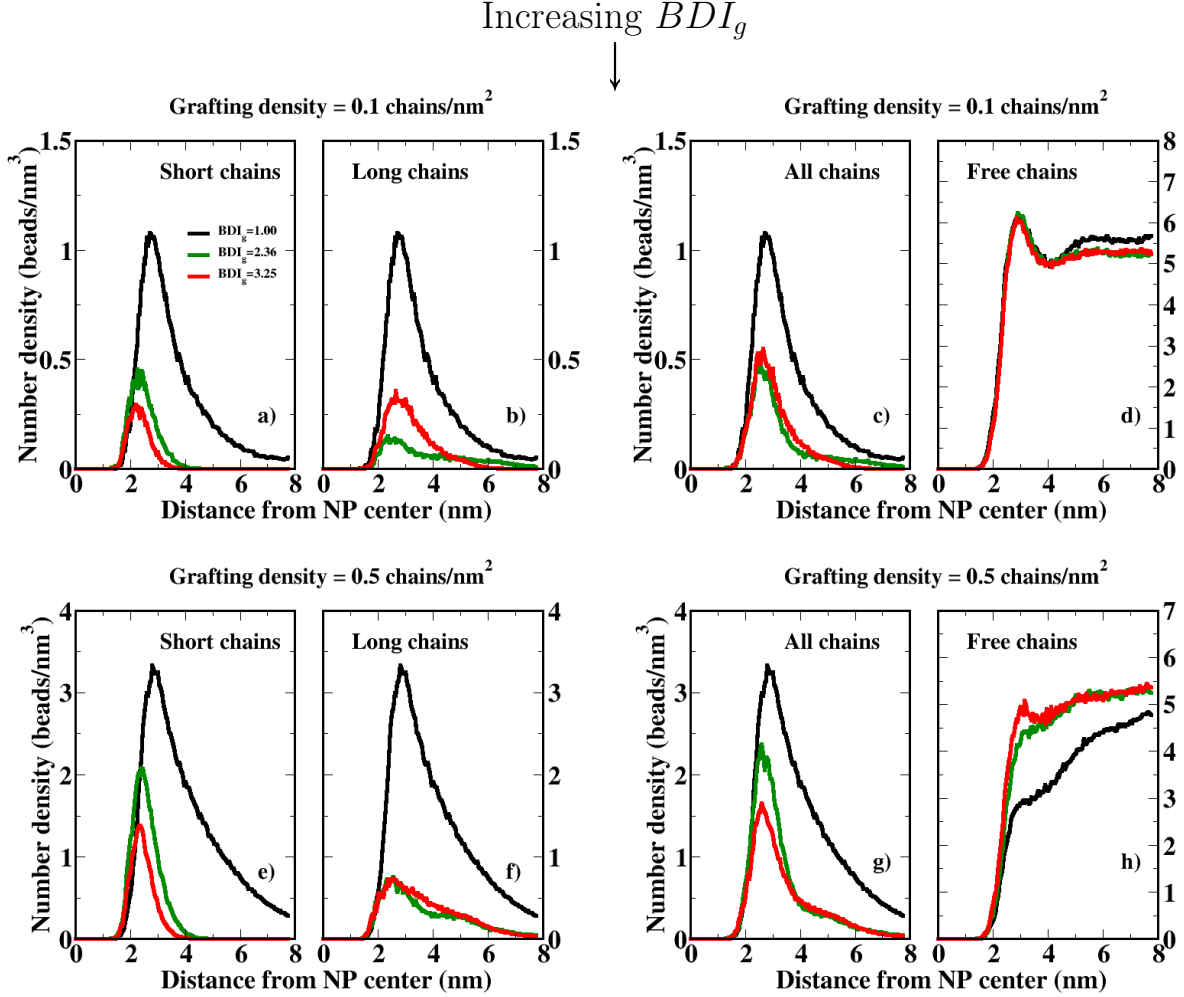


Figure 8: Radial number density of monomers belonging to grafted and free chains. Two different grafting densities, namely $\rho_g = 0.1$ (top panels) and 0.5 (bottom panels) chains/nm² are reported. Short, long and all grafted chains are separately shown.

the corresponding profile of long chains and the distribution of all grafted chains (panel (g)) shows a dependence on BDI_g , decreasing when the latter increases. The reverse behavior is found for free chains (panel (h)).

The two-body PMF as a function of BDI_g is shown in Fig. 9. It is worth pointing out that, as anticipated in the **System preparation** subsection, for bidisperse grafted chains a dependence on M_n can be expected; hence, we have also calculated the two-body PMF for $\rho_g = 0.1$ and 0.5 chains/nm² keeping this quantity constant. For $\rho_g = 0.1$ chains/nm² (panel (a)), upon increasing BDI_g a non-monotonic increase of the repulsion between the

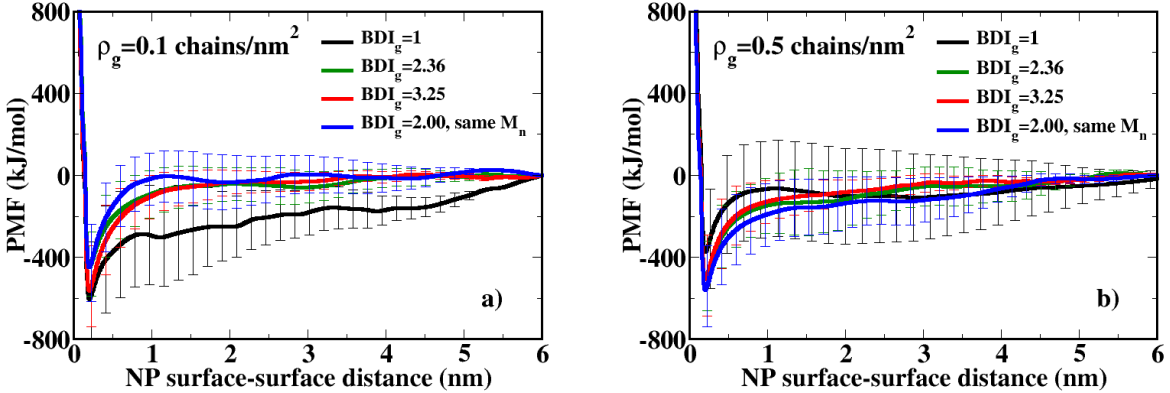


Figure 9: Effect of increasing the bidispersity index of grafted chains on the potential of mean force between two grafted nanoparticles with grafting density $\rho = 0.1$ (a) and 0.5 (b) chains/nm². In all cases the free chains are monodisperse.

two NPs is found. This repulsion becomes stronger for $BDI_g = 2.36$ than for $BDI_g = 3.25$. A comparison with the corresponding monomer number density (see panels (a) and (b) of Fig. 8) suggests that the PMF is more repulsive if the arrangement of long grafted chains around the NP surface worsens (in comparison with the monodisperse case) and vice versa. The non-monotonic behavior of the PMF upon increasing BDI_g also suggests that in this case two different effects (attraction due to the decrease of the length of the grafted chains, and repulsion due to the increase of the wettability) compete, giving rise to a PMF slightly more repulsive than in the monodisperse case, but still exhibiting an attractive well for short interparticle separations. These effects can be ascribed almost entirely to the increase of BDI_g ; indeed, the behavior of the PMF calculated for $BDI_g = 2.00$, with M_n kept constant, is very similar to those already discussed. It is worth comparing the results obtained so far with an experimental study devoted to investigate the influence of the polydispersity of the grafted chains on the behavior of silica-PS nanocomposites in the case of low grafting densities.¹¹ It is known that for monodisperse distributions of free and grafted PS chains and low grafting densities, NPs can self-assemble in a large variety of different super-structures, including strings, connected sheets or small clusters.⁸ Upon comparing their

results with those already existing for monodisperse polymer chains¹ the authors observe that for bidisperse grafted chains the NPs appear well dispersed in a more extended region of the phase diagram. Hence, they suggest that a good recipe for increasing the repulsion between grafted NPs is to use a bidisperse distribution of grafted PS chains, as in the present case. Our results are in agreement with these experimental findings. Interestingly, a similar behavior was observed also in an earlier Monte Carlo study of the bidispersity in the length of the grafted chains and its effects on the PMF between NPs in homopolymer melts.⁵⁸ Indeed in that work the authors found that the repulsion between NPs increases with BDI_g . A subsequent theoretical-simulation study¹⁶ has shown that NPs with bidisperse distributions where the number of long grafted chains is less than the number of short grafted chains (*i.e.* the same prescription adopted in the present work) is more efficient in stabilizing the nanocomposites against the aggregation in comparison to both unimodal and polydisperse distributions. Finally, by looking at the behavior of the two-body PMF for $BDI_f = 2.36$ (Fig. 6a) and for $BDI_g = 2.36$ and 3.25 (Fig. 9a) we also observe the existence of a short-range attraction followed by a repulsion for intermediate NP-NP separation: as described in Ref.,²⁴ this picture is compatible with the onset of self-assembled structures in the system, as also experimentally detected.^{1,2,8}

The effect of increasing BDI_g on the PMF between two grafted NPs for $\rho_g = 0.5$ chains/nm² is presented in Fig. 9b. Unlike all cases documented so far, the increase of BDI_g generates an increase of the attraction between the NPs. Indeed, since now the grafting density is higher, the free chains hardly penetrate the grafted corona and the wettability is low; on the other hand, the reduction of the grafted chain length upon increasing BDI_g is significant (see Tab. 2) and hence the attractive contribution to the PMF is dominant. As observed for $\rho_g = 0.1$ chains/nm², also in this case the differences with respect to the unimodal distribution can be attributed to the increase of the bidispersity, rather than to the different values of M_n . Note that in all cases the PMF is entirely attractive and no nanostructured aggregate can be expected. This is confirmed by experiments² and simula-

tion¹ studies, where it was found that complex aggregates are observed only for low grafting densities (i.e. 0.1 chains/nm²), whereas only phase separation or well dispersed conditions can be expected for intermediate-to-high grafting densities.

Summarizing the pictures emerging from Fig. 6a and 9a it appears that a good strategy for obtaining a well dispersed state for $\rho_g = 0.1$ chains/nm² is to significantly increase the bidispersity of free chains, leaving BDI_g unchanged. On the other hand, a moderate increase of BDI_f or BDI_g may allow the system to have an onset of more complex structures, not observed in the monodisperse case. Further information on the role played by the wettability is gained by calculating the penetration depth of the free chains into the grafted corona: this quantity shows a noticeable correlation with the behavior of the two-body PMF (see the **S.I.**).

Expected phase behavior

The phase behavior of the nanocomposite can be further characterized by calculating the second virial coefficient B_2 from the PMF; in particular, it is known that positive values of B_2 indicate that repulsive contributions are dominant, whereas its negative values suggest a prevalence of attractive interactions.⁵⁹ This circumstance sets the second virial coefficient as a suitable tool for quickly predicting the changes in the phase behavior of self-assembling systems.^{60,61} The general definition of the second virial coefficient for a potential without an angular dependence can be written as:⁶²

$$B_2 = 2\pi \int_0^\infty (1 - e^{-\beta U(r)}) r^2 dr, \quad (9)$$

where $U(r)$ is the PMF, $\beta = 1/k_B T$ and r is the interparticle separation. In our case the interval of integration $[0, \infty]$ is replaced by $[d_{\min}, d_{\max}]$ according to the definition of Eq. 3. It may be worth pointing out that the calculation of B_2 can not discriminate between a phase separation and the onset of aggregation, since in both cases $B_2 < 0$. However the behavior of

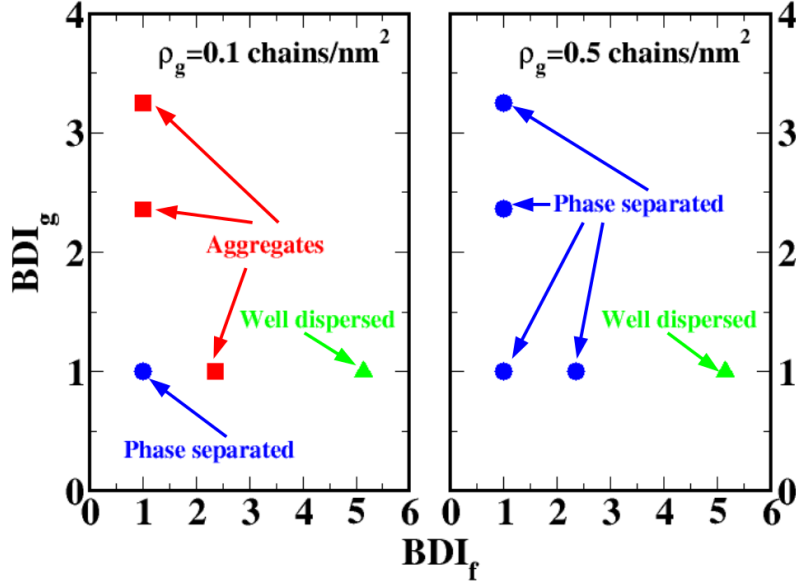


Figure 10: Schematic phase behavior of grafted nanoparticles as a function of bidispersity and grafting density. The diagram is drawn by considering the behavior of the two-body PMF and the second virial coefficient. Different colors and symbols identify phase separated ($B_2 < 0$), aggregated ($B_2 < 0$) and well dispersed ($B_2 > 0$) conditions.

the PMF is different in these two situations, since in the first case it is attractive in the whole range of interparticle separations, whereas in the second case it is short-range attractive and long-range repulsive, as largely documented in literature.^{63–65} The resulting, schematic, phase diagram is reported in Fig. 10: it clearly emerges that for $\rho_g = 0.1$ chains/nm², the increase of BDI_f or BDI_g causes a corresponding increase of the repulsion, favouring the onset of aggregates or well dispersed conditions that replace the phase separation observed in the monodisperse case. On the other hand, for $\rho_g = 0.5$ chains/nm² the phase separation still persists upon increasing BDI_g and only a large BDI_f leads to well-dispersed conditions.

These effects are expected to be even more significant if multi-body contributions to the PMF are taken into account. In order to ascertain the importance of these contributions, we present in the next section results obtained by calculating the three-body PMF, comparing them with the two-body case and the experimental data.

Table 3: Nanocomposite systems investigated for the calculation of the three-body potential of mean force. The grafting density ρ_g is in unit of chains/nm². The chains length is given in number of beads. The box lengths are $L_x = L_y = L_z = 22$ nm.

| ρ_g | No° of short grafted chains | No° of long grafted chains | Short grafted chains length | Long grafted chains length | No° of short free chains | No° of long free chains | Short free chains length | Long free chains length | BDI_g | BDI_f |
|----------|-----------------------------|----------------------------|-----------------------------|----------------------------|--------------------------|-------------------------|--------------------------|-------------------------|---------|---------|
| 0 | 0 | 0 | 0 | 0 | 2796 | 0 | 20 | 0 | 1 | 1 |
| 0 | 0 | 0 | 0 | 0 | 2200 | 60 | 20 | 200 | 1 | 2.36 |
| 0.1 | 0 | 5 | 0 | 80 | 2775 | 0 | 20 | 0 | 1 | 1 |
| 0.1 | 0 | 5 | 0 | 80 | 2178 | 60 | 20 | 200 | 1 | 2.36 |
| 0.1 | 0 | 5 | 0 | 80 | 264 | 50 | 20 | 1000 | 1 | 5.14 |
| 0.1 | 4 | 1 | 10 | 80 | 2775 | 0 | 20 | 0 | 2.36 | 1 |
| 0.1 | 4 | 1 | 5 | 80 | 2775 | 0 | 20 | 0 | 3.25 | 1 |
| 0.1 | 4 | 1 | 80 | 1000 | 2595 | 0 | 20 | 0 | 2.94 | 1 |
| 0.5 | 0 | 25 | 0 | 80 | 2527 | 0 | 20 | 0 | 1 | 1 |
| 0.5 | 0 | 25 | 0 | 80 | 1987 | 54 | 20 | 200 | 1 | 2.36 |
| 0.5 | 20 | 5 | 10 | 80 | 2691 | 0 | 20 | 0 | 2.36 | 1 |

Three-body potential of mean force

The complete collection of systems investigated for the calculation of the three-body PMF is shown in Tab. 3. The simulation box is now cubic in order to allow a proper arrangement of the third NP to occur. In Fig. 11 we compare three-body and two-body PMFs between ungrafted NPs for $BDI_f = 1.00$ and $BDI_f = 2.36$. It emerges that the three-body PMF is remarkably more attractive than the simpler two-body interaction, due to the presence of the third NP in close contact with the first two. This behavior holds regardless of the bidispersity and is primarily due to the fact that a very low number of chains can be arranged between the NPs, as explained also in Ref.²⁴ Also, the oscillations observed in the two-body PMF disappear in the three-body interaction: this is due to the perturbation caused by the third NP to the previously described mechanism of association, which gives rise to an attraction monotonically increasing upon decreasing the interparticle distance.

Since the most interesting phase behaviors are observed for $\rho_g = 0.1$ chains/nm², due to the possible appearance of self-assembled structures, we investigate this specific grafting

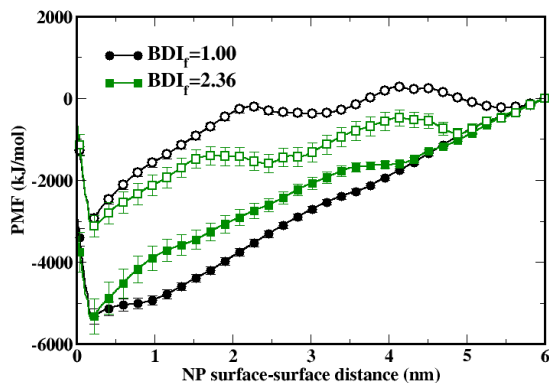


Figure 11: Comparison between three-body (full symbols) and two-body (open symbols) potential of mean force between ungrafted nanoparticles upon increasing the bidispersity index of the free chains.

density in more detail. In Fig. 12a we report the three-body PMF for $\rho_g = 0.1$ chains/nm² upon increasing BDI_f , comparing the results with the two-body PMF obtained in the same conditions (see Fig. 6a). In the monodisperse case, as also observed in Ref.,²⁴ the three-body PMF is remarkably more repulsive than the two-body counterpart; for $BDI_f = 2.36$ the trend appears reversed, whereas upon increasing BDI_f to 5.14, two- and three-body PMFs similarly behave. Hence, it appears that the multi-body effects and the increased wettability of the NPs surface are combined in a non-trivial way, giving rise to an effective interaction which is non-monotonically dependent on the bidispersity. Furthermore, the differences between two- and three-body PMFs are progressively less pronounced upon increasing BDI_f . Interestingly, we finally note that the three-body cases studied are compatible with systems where self-assembled structures arise, as experimentally expected.

The effect of increasing BDI_g on the three-body PMF is analyzed in Fig. 12b, along with the comparison with the two-body case. As already observed upon increasing BDI_f , the effect of the bidispersity on the three-body PMF is less evident than in the two-body counterpart: this is indicated by the similarity between all the three-body PMF profiles. On the other hand, in all cases the repulsion increases when going from the two-body to the three-

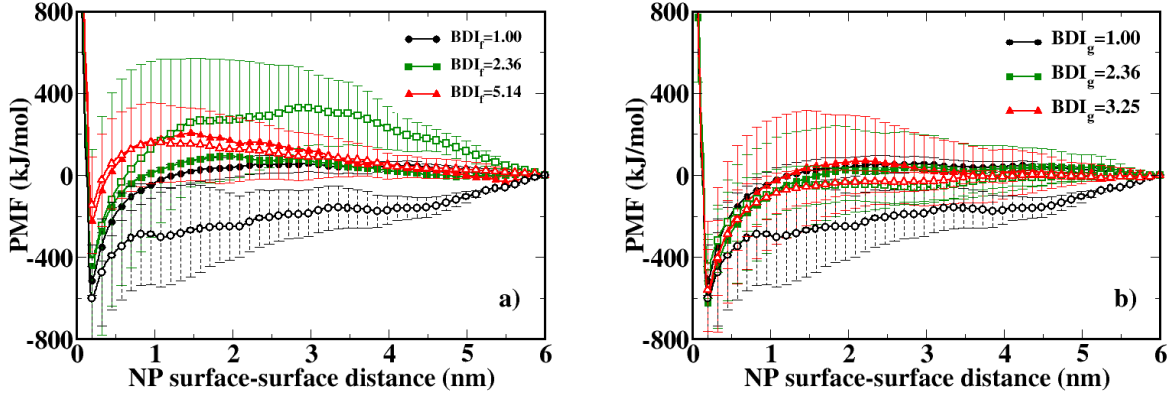


Figure 12: Panel (a): comparison between three-body (full symbols) and two-body (open symbols) potentials of mean force between grafted nanoparticles with grafting density $\rho_g=0.1$ chains/nm² upon increasing the bidispersity index of free chains. In all cases the grafted chains are monodisperse. Panel (b): same as panel (a) upon increasing the bidispersity index of the grafted chains, while the free chains are monodisperse.

body interaction. This finding is in agreement with the results obtained for monodisperse systems²⁴ and also supports previously discussed experimental studies¹¹ where it was stated that a good way for obtaining a good dispersion of NPs in the composite is to increase BDI_g , provided that the grafting density is low.

However, even if the three-body PMF is more repulsive than its two-body counterpart, a good dispersion is not reached, since the effective interaction still exhibits a deep attractive well. In this context it is worth noting that in the calculation of the multi-body contributions to the PMF, M_n of the grafted chains is expected to play a more significant role than in the two-body case.²⁴ Hence, since for both BDI_g investigated so far, M_n has been decreased, we have performed further simulations for $BDI_g = 2.94$ (see Tab. 3) where M_n has been increased. The results, reported in the **S.I.**, indicate that under these conditions the three-body PMF is almost entirely repulsive and compatible with a well dispersed condition.

Finally, in Fig. 13 we analyze the effect of the bidispersity on the three-body PMF for $\rho_g = 0.5$ chains/nm². In this case the three-body PMF is systematically more repulsive than the two-body interaction upon increasing both BDI_f and BDI_g . This is due to the

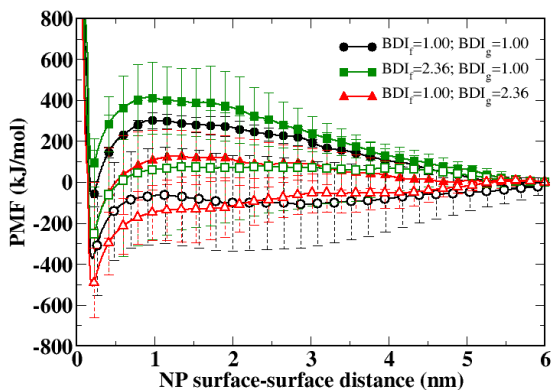


Figure 13: Comparison between three-body (full symbols) and two-body (open symbols) potentials of mean force between grafted nanoparticles with grafting density $\rho_g = 0.5$ chains/nm² upon increasing the bidispersity index of free and grafted chains.

repulsion between the grafted chains, which increases if a third NP is placed close to the first two. Interestingly, the increase of BDI_f promotes the repulsion, while the increase of BDI_g favours the attraction: this picture holds both for the two-body and the three-body PMFs. This finding suggests that for this grafting density the mechanisms governing the microscopic interactions are maintained when going from a two-body to a three-body description of the PMF.

The refinement of the simpler two-body interactions and the qualitative agreement with the experimental results confirm that the multi-body effects are not negligible in polymer nanocomposites, and that a proper tuning of the bidispersity can be useful in view of obtaining a desired structure.

Conclusions

In the present work we have studied the local structure and the effective interactions in a polymer nanocomposite system constituted by silica nanoparticles (NPs) in a polystyrene (PS) melt. NPs are assumed to be either bare or grafted with PS chains. The study has

been performed by applying the hybrid particle-field molecular dynamics approach, which has allowed us to successfully simulate even systems with high molecular weight PS chains. The main focus of our investigation concerned the role played by the bidispersity of the length of the polymer chains in determining the final phase behavior of the composite system. A comparison with previous atomistic^{41,42,57} and coarse-grained⁴⁰ molecular dynamics simulation studies concerning monodisperse systems has shown a good agreement in reproducing the local structure of polymer chains around the NPs. By calculating the monomer number densities of both free and grafted chains and the two- or multi-body potentials of mean force (PMF) we have ascertained that if the NPs are ungrafted, an increase of the bidispersity index (BDI) causes a stronger attraction between them. In the grafted cases, a crucial role is played by the grafting density ρ_g : for $\rho_g = 0.1$ chains/nm² the increase of BDI of both free and grafted chains (BDI_f and BDI_g , respectively) causes a rise of the repulsion between the NPs. Instead, for $\rho_g = 0.5$ chains/nm² the repulsion increases only with BDI_f and diminishes if BDI_g increases. It is worth noting that some trends observed in the present study (such as the attraction between the ungrafted NPs and the increase of the repulsion with the grafting density of grafted NPs) are not limited to the specific case of silica-PS nanocomposites but are quite general. The complex interplay between bidispersity, grafting density and multi-body interaction gives rise to a rich phase behavior which qualitatively follows the available experimental data on these systems. The capability of the hybrid particle-field approach to describe the microscopic interactions at the molecular level sets this method as a valuable tool for investigations of the composite stability under a large variety of conditions.

Supporting Information

Calculation of the penetration depth of free chains inside the grafted corona of a nanoparticle as a function of grafting density and bidispersity; calculation of the three-body potential of

mean force between nanoparticles grafted by polymer chains with high molecular weight.

Acknowledgements

The computing resources and the related technical support used for this work have been provided by CRESCO/ENEAGRID High Performance Computing infrastructure and its staff.⁶⁶ CRESCO/ENEAGRID High Performance Computing infrastructure is funded by ENEA, the Italian National Agency for New Technologies, Energy and Sustainable Economic Development and by Italian and European research programs, see <http://www.cresco.enea.it/english> for information. Gianmarco Munaò and Giuseppe Milano acknowledge financial support from the European Union Horizon 2020 Programme, under Grant Agreement No. 760940. Andreas Kalogirou and Florian Müller-Plathe acknowledge support by the Deutsche Forschungsgemeinschaft through the Collaborative Research Centre Transregio 146 ‘Multiscale Simulation Methods for Soft-Matter Systems.’

References

- (1) Akcora, P.; Liu, H.; Kumar, S. K.; Moll, J.; Li, Y.; Benicewicz, B. C.; Schadler, L. S.; Acechin, D.; Panagiotopoulos, A. Z.; Pyramitsyn, V.; Ganesan, V.; Ilavsky, J.; Thiyagarajan, P.; Colby, R. H.; Douglas, J. F. Anisotropic self-assembly of spherical polymer-grafted nanoparticles. *Nat. Mater.* **2009**, *8*, 354–359.
- (2) Akcora, P.; Kumar, S. K.; Moll, J.; Lewis, S.; Schadler, L. S.; Li, Y.; Benicewicz, B. C.; Sandy, A.; Narayanan, S.; Ilavsky, J.; Thiyagarajan, P.; Colby, R. H.; Douglas, J. F. ‘Gel-like’ mechanical reinforcement in polymer nanocomposite melts. *Macromolecules* **2010**, *43*, 1003–1010.
- (3) Kumar, S. K.; Ganesan, V.; Riggleman, R. A. Perspective: Outstanding theoretical questions in polymer-nanoparticle hybrids. *J. Chem. Phys.* **2017**, *147*, 020901.

- (4) Lan, Q.; Francis, L. F.; Bates, F. S. Silica nanoparticle dispersions in homopolymer versus block copolymer. *J. Polym. Sci., Polym. Phys.* **2007**, *45*, 2284–2299.
- (5) Chevigny, C.; Jestin, J.; Gimes, D.; Schweins, R.; Di Cola, E.; Dalmas, F.; Bertin, D.; Bouè, F. “Wet-to-Dry” Conformational Transition of Polymer Layers Grafted to Nanoparticles in Nanocomposite. *Macromolecules* **2010**, *43*, 4833–4837.
- (6) Sunday, D.; Ilavsky, J.; Green, D. L. A Phase Diagram for Polymer-Grafted Nanoparticles in Homopolymer Matrices. *Macromolecules* **2012**, *45*, 4007–4011.
- (7) Srivastava, S.; Agarwal, P.; Archer, L. A. Tethered nanoparticle-polymer composites: phase stability and curvature. *Langmuir* **2012**, *28*, 6276–6281.
- (8) Kumar, S. K.; Jouault, N.; Benicewicz, B.; Neely, T. Nanocomposites with Polymer Grafted Nanoparticles. *Macromolecules* **2013**, *46*, 3199–3214.
- (9) Park, S. J.; Kim, S.; Yong, D.; Choe, Y.; Bang, J.; Kim, J. U. Interactions between brush-grafted nanoparticles within chemically identical homopolymers: the effect of brush polydispersity. *Soft Matter* **2018**, *14*, 1026–1042.
- (10) Rungta, A.; Natarajan, B.; Neely, T.; Dukes, D.; Schadler, L. S.; Benicewicz, B. C. Grafting Bimodal Polymer Brushes on Nanoparticles Using Controlled Radical Polymerization. *Macromolecules* **2012**, *45*, 9303–9311.
- (11) Natarajan, B.; Neely, T.; Rungta, A.; Benicewicz, B. C.; Schadler, L. S. Thermomechanical Properties of Bimodal Brush Modified Nanoparticle Composites. *Macromolecules* **2013**, *46*, 4909–4918.
- (12) Li, Y.; Tao, P.; Viswanath, A.; Benicewicz, B. C.; Schadler, L. S. Bimodal Surface Ligand Engineering: The Key to Tunable Nanocomposites. *Langmuir* **2013**, *29*, 1211–1220.

- (13) Triebel, C.; Kunzelmann, P.; Blankeburg, M.; Münstedt, H. Elasticity of polystyrene melts filled with silica nanoparticles: Influence of matrix polydispersity. *Polymer* **2011**, *52*, 3621–3626.
- (14) Dodd, P. M.; Jayaraman, A. Monte Carlo Simulations of Polydisperse Polymers Grafted on Spherical Surfaces. *J. Polym. Sci. B* **2012**, *50*, 694–705.
- (15) Martin, T. B.; Dodd, P. M.; Jayaraman, A. Polydispersity for Tuning the Potential of Mean Force between Polymer Grafted Nanoparticles in a Polymer Matrix. *Phys. Rev. Lett.* **2013**, *110*, 018301.
- (16) Martin, T. B.; Jayaraman, A. Identifying the Ideal Characteristics of the Grafted Polymer Chain Length Distribution for Maximizing Dispersion of Polymer Grafted Nanoparticles in a Polymer Matrix. *Macromolecules* **2013**, *46*, 9144–9150.
- (17) Martin, T. B.; Jayaraman, A. Polydisperse homopolymer grafts stabilize dispersions of nanoparticles in a chemically identical homopolymer matrix: an integrated theory and simulation study. *Soft Matter* **2013**, *9*, 6876–6889.
- (18) Martin, T. B.; Jayaraman, A. Effect of Matrix Bidispersity on the Morphology of Polymer-Grafted Nanoparticle-Filled Polymer Nanocomposites. *J. Polym. Sci. B* **2014**, *52*, 1661–1668.
- (19) Langeloth, M.; Masubuchi, Y.; Böm, M. C.; Müller-Plathe, F. Reptation and constraint release dynamics in bidisperse polymer melts. *J. Chem. Phys.* **2014**, *141*, 194904.
- (20) Shi, R.; Qian, H.-J.; Lu, Z.-Y. Computer simulation study on the self-assembly of unimodal and bimodal polymer-grafted nanoparticles in a polymer melt. *Phys. Chem. Chem. Phys.* **2017**, *19*, 16524.
- (21) Mathioudakis, I. G.; Vogiatzis, G. G.; Tzoumanekas, C.; Theodorou, D. N. Multiscale

- simulations of PS-SiO₂ nanocomposites: from melt to glassy state. *Soft Matter* **2016**, *12*, 7585–7605.
- (22) Vogiatzis, G. G.; Theodorou, D. N. Structure of Polymer Layers Grafted to Nanoparticles in Silica-Polystyrene Nanocomposites. *Macromolecules* **2013**, *46*, 4670–4683.
- (23) Vogiatzis, G. G.; Voyiatzis, E.; Theodorou, D. N. Monte Carlo simulations of a coarse grained model for an athermal all-polystyrene nanocomposite system. *Eur. Polym. J.* **2011**, *47*, 699–712.
- (24) Munaò, G.; Pizzirusso, A.; Kalogirou, A.; De Nicola, A.; Kawakatsu, T.; Müller-Plathe, F.; Milano, G. Molecular Structure and Multi-Body Interactions in Silica-Polystyrene Nanocomposites. *Nanoscale* **2018**, *10*, 21656–21670.
- (25) Frischknecht, A. L.; Yethiraj, A. Two- and three-body interactions among nanoparticles in a polymer melt. *J. Chem. Phys.* **2011**, *134*, 174901.
- (26) Milano, G.; Kawakatsu, T. Hybrid particle-field molecular dynamics simulations for dense polymer systems. *J. Chem. Phys.* **2009**, *130*, 214106.
- (27) De Nicola, A.; Avolio, R.; Della Monica, F.; Gentile, G.; Cocca, M.; Capacchione, C.; Errico, M. E.; Milano, G. Rational design of nanoparticle/monomer interfaces: a combined computational and experimental study of in situ polymerization of silica based nanocomposites. *RSC Advances* **2015**, *5*, 71336–71340.
- (28) De Nicola, A.; Kawakatsu, T.; Müller-Plathe, F.; Milano, G. Fast relaxation of coarse-grained models of polymer interphases by hybrid particle-field molecular dynamics: Polystyrene-silica nanocomposites as an example. *Eur. Phys. J. Special Topics* **2016**, *225*, 1817–1841.
- (29) De Nicola, A.; Kawakatsu, T.; Milano, G. Generation of Well Relaxed All Atom Models of Large Molecular Weight Polymer Melts: A Hybrid Particle-Continuum Approach

- Based on Particle-Field Molecular Dynamics Simulations. *J. Chem. Theory Comput.* **2014**, *10*, 5651–5667.
- (30) Zhao, Y.; Byshkin, M.; Cong, Y.; Kawakatsu, T.; Guadagno, L.; De Nicola, A.; Yu, N. S.; Milano, G.; Dong, B. Self-Assembly of Carbon Nanotubes in Polymer Melts: Simulation of Structural and Electrical Behaviour by Hybrid Particle-Field Molecular Dynamics. *Nanoscale* **2016**, *8*, 15538–15552.
- (31) Sgouros, A. P.; Megariotis, G.; Theodorou, D. N. Slip-Spring Model for the Linear and Nonlinear Viscoelastic Properties of Molten Polyethylene Derived from Atomistic Simulations. *Macromolecules* **2017**, *50*, 4524–4541.
- (32) Vogiatzis, G. G.; Megariotis, G.; Theodorou, D. N. Equation of State Based Slip Spring Model for Entangled Polymer Dynamics. *Macromolecules* **2017**, *50*, 3004–3029.
- (33) Megariotis, G.; Vogiatzis, G. G.; Sgouros, A. P.; Theodorou, D. N. Slip Spring-Based Mesoscopic Simulations of Polymer Networks: Methodology and the Corresponding Computational Code. *Polymers* **2018**, *10*, 1156.
- (34) Sgouros, A. P.; Lakkas, A. T.; Megariotis, G.; Theodorou, D. N. Mesoscopic Simulations of Free Surfaces of Molten Polyethylene: Brownian Dynamics/Kinetic Monte Carlo Coupled with Square Gradient Theory and Compared to Atomistic Calculations and Experiment. *Macromolecules* **2018**, *51*, 9798–9815.
- (35) De Nicola, A.; Kawakatsu, T.; Rosano, C.; Celino, M.; Rocco, M.; Milano, G. Self-Assembly of Triton X-100 in Water Solutions: A Multiscale Simulation Study Linking Mesoscale to Atomistic Models. *J. Chem. Theory Comp.* **2015**, *11*, 4959–4971.
- (36) De Nicola, A.; Zhao, Y.; Kawakatsu, T.; Roccatano, D.; Milano, G. Hybrid Particle-Field Coarse-Grained Models for Biological Phospholipids. *J. Chem. Theory Comp.* **2011**, *11*, 2947–2962.

- (37) Bore, S.; Milano, G.; Cascella, M. Hybrid Particle-Field Model for Conformational Dynamics of Peptide Chains. *J. Chem. Theory Comp.* **2018**, *14*, 1120–1130.
- (38) De Nicola, A.; Hezaveh, S.; Kawakatsu, T.; Roccatano, D.; Milano, G. Micellar drug nanocarriers and biomembranes: how do they interact? *Phys. Chem. Chem. Phys.* **2014**, *16*, 5093–5105.
- (39) Qian, H.-J.; Carbone, P.; Chen, X.; Karimi-Varzaneh, H. A.; Liew, C. C.; Müller-Plathe, F. Temperature-Transferable Coarse-Grained Potentials for Ethylbenzene, Polystyrene, and Their Mixtures. *Macromolecules* **2008**, *41*, 9919–9929.
- (40) Ghanbari, A.; Nodoro, T. V. M.; Leroy, F.; Rahimi, M.; Böhm, M. C.; Müller-Plathe, F. Interphase Structure in Silica-Polystyrene Nanocomposites: A Coarse-Grained Molecular Dynamics Study. *Macromolecules* **2012**, *45*, 572–584.
- (41) Nodoro, T. V. M.; Voyiatzis, E.; Ghanbari, A.; Theodorou, D. N.; Böhm, M. C.; Müller-Plathe, F. Interface of Grafted and Ungrafted Silica Nanoparticles with a Polystyrene Matrix: Atomistic Molecular Dynamics Simulations. *Macromolecules* **2011**, *44*, 2316–2327.
- (42) Nodoro, T. V. M.; Böhm, M. C.; Müller-Plathe, F. Interface and Interphase Dynamics of Polystyrene Chains near Grafted and Ungrafted Silica Nanoparticles. *Macromolecules* **2012**, *45*, 171–179.
- (43) Kawakatsu, T. *Statistical Physics of Polymers*; Springer: Berlin, 2004.
- (44) Zhao, Y.; De Nicola, A.; Kawakatsu, T.; Milano, G. Hybrid particle-field molecular dynamics simulations: Parallelization and benchmarks. *J. Comput. Chem.* **2012**, *33*, 868–880.
- (45) Martinez, L.; Andrade, R.; Birgin, E. G.; Martinez, J. M. PACKMOL: A package for

- building initial configurations for molecular dynamics simulations. *J. Comput. Chem.* **2009**, *30*, 2157–2164.
- (46) Sides, S. W.; Kim, B. J.; Kramer, E. J.; Fredrickson, G. H. Hybrid particle-field simulations of polymer nanocomposites. *Phys. Rev. Lett.* **2006**, *96*, 250601.
- (47) Hooper, J. B.; Schweizer, K. S.; Desai, T. G.; Koshy, R.; Keblinski, P. Structure, surface excess and effective interactions in polymer nanocomposite melts and concentrated solutions. *J. Chem. Phys.* **2004**, *121*, 6986.
- (48) Hamaker, H. C. The London-van der Waals attraction between spherical particles. *Physica* **1937**, *4*, 1058–1072.
- (49) Munaò, G.; Correa, A.; Pizzirusso, A.; Milano, G. On the calculation of the potential of mean force between atomistic nanoparticles. *EPJ E* **2018**, *41*, 38.
- (50) Hooper, J. B.; Schweizer, K. S. Contact Aggregation, Bridging, and Steric Stabilization in Dense Polymer-Particle Mixtures. *Macromolecules* **2005**, *38*, 8858–8869.
- (51) Bedrov, D.; Smith, G. D.; Smith, J. S. Matrix-induced nanoparticle interactions in a polymer melt: A molecular dynamics simulation study. *J. Chem. Phys.* **2003**, *119*, 10438.
- (52) Milano, G.; Müller-Plathe, F. Cyclohexane-Benzene Mixtures: Thermodynamics and Structure from Atomistic Simulations. *J. Phys. Chem. B* **2004**, *108*, 7415–7423.
- (53) Green, P. F. The structure of chain end-grafted nanoparticle/homopolymer nanocomposites. *Soft Matter* **2011**, *7*, 7914–7926.
- (54) Trombly, D. M.; Ganesan, V. Curvature effects upon interactions of polymer-grafted nanoparticles in chemically identical polymer matrices. *J. Chem. Phys.* **2010**, *133*, 154904.

- (55) Pronk, S.; Pall, S.; Schulz, R.; Larsson, P.; Bjelkmar, P.; Apostolov, R.; Shirts, M. R.; Smith, J. C.; Kasson, P. M.; van der Spoel, D.; Hess, B.; Lindahl, E. GROMACS 4.5: a high-throughput and highly parallel open source molecular simulation toolkit. *Bioinformatics* **2013**, *29*, 845–854.
- (56) Mortezaei, M.; Famili, M. H. N.; Kokabi, M. The role of interfacial interactions on the glass-transition and viscoelastic properties of silica/polystyrene nanocomposite. *Compos. Sci. Technol.* **2011**, *7*, 1039–1045.
- (57) Eslami, H.; Rahimi, M.; Müller-Plathe, F. Molecular Dynamics Simulation of a Silica Nanoparticle in Oligomeric Poly(methyl methacrylate): A Model System for Studying the Interphase Thickness in a Polymer-Nanocomposite via Different Properties. *Macromolecules* **2013**, *46*, 8680–8692.
- (58) Nair, N.; Wentzel, N.; Jayaraman, A. Effect of bidispersity in grafted chain length on grafted chain conformations and potential of mean force between polymer grafted nanoparticles in a homopolymer matrix. *J. Chem. Phys.* **2011**, *134*, 194906.
- (59) Hansen, J. P.; McDonald, I. R. *Theory of simple liquids*, 3rd Ed.; Academic Press, New York, 2006.
- (60) Munaò, G.; O’Toole, P.; Hudson, T. S.; Costa, D.; Caccamo, C.; Sciortino, F.; Giacometti, A. Cluster formation and phase separation in heteronuclear Janus dumbbells. *J. Phys.: Condens. Matter* **2015**, *27*, 234101.
- (61) Prestipino, S.; Munaó, G.; Costa, D.; Caccamo, C. Self-assembly in a model colloidal mixture of dimers and spherical particles. *J. Chem. Phys.* **2017**, *146*, 084902.
- (62) McQuarrie, D. A. *Statistical Mechanics*; Harper Collins, New York, 1976.
- (63) Stradner, A.; Sedgwick, H.; Cardinaux, F.; Poon, W. C.; Egelhaaf, S. U.; Schurten-

- berger, P. Equilibrium cluster formation in concentrated protein solutions and colloids. *Nature* **2004**, *432*, 492–495.
- (64) Sciortino, F.; Mossa, S.; Zaccarelli, E.; Tartaglia, P. Equilibrium Cluster Phases and Low-Density Arrested Disordered States: The Role of Short-Range Attraction and Long-Range Repulsion. *Phys. Rev. Lett.* **2004**, *93*, 055701.
- (65) Liu, Y.; Porcar, L.; Chen, J.; Chen, W.-R.; Falus, P.; Faraone, A.; Fratini, E.; Hong, K.; Baglioni, P. Lysozyme protein solution with an intermediate range order structure. *J. Phys. Chem. B* **2011**, *115*, 7238–7247.
- (66) Ponti, G.; et al, The role of medium size facilities in the HPC ecosystem: the case of the new CRESCO4 cluster integrated in the ENEAGRID infrastructure. *Proceedings of the 2014 International Conference on High Performance Computing and Simulation* **2014**, *6903807*, 1030.